Application of Immersed Boundary Method for Flow Over Stationary and Oscillating Cylinders

Dae Sung Lee, Man Yeong Ha*, Sung Jin Kim
Department of mechanical engineering, Pusan National University, Busan 609-735, Korea
Hyun Sik Yoon
ASERC, Pusan National University, Busan 609-375, Korea

IBM (Immersed Boundary Method) with feedback momentum forcing was applied to stationary and moving bodies. The capability of IBM to treat the obstacle surfaces, especially with moving effect has been tested for two dimensional problems. Stationary and oscillating cylinders were simulated by using IBM based on finite volume method with Cartesian coordinates. For oscillating cylinder, lateral and vertical motions are considered, respectively. Present results such as time histories of drag and lift coefficients for both stationary and oscillating cases are in good agreement with previous numerical and experimental results. Also, the instantaneous wake patterns of oscillating cylinder with different oscillating frequency ratios well represented those of previous researches. More feasibility study for IBM has been carried out to two oscillating cylinders. Drag and lift coefficients are presented for two cylinders oscillating sinusoidally with phase difference of 180°.

Key Words : Immersed Boundary Method, Oscillating Cylinder, Drag & Lift Coefficients

Nomenclature

A_e : Amplitude of oscillating cylinder
$D_{i,j}(x_s)$: Bilinear interpolation function
D : Diameter of cylinder
$F(x_s, t)$: Forcing density
F : Dimensionless in-line force
f : Momentum forcing added to momentum equation
f_e : Oscillation frequency
f_m : Modulation frequency
f_o : Strouhal number of fixed cylinder
g : Dimensionless gap between cylinders
KC : Keulegan-Carpenter number, $U_{\max}/f_eD$
n : Number of neighboring immersed boundary points
Re : Reynolds number, $U_\infty D/\nu$, for fixed and cross flow oscillating cylinder
Re_{cyl} : Reynolds number, $U_{\max}D/\nu$, for inline oscillating flow
St : Strouhal number, fD/U_∞
t : Dimensionless time
T_e : Oscillation period, $1/f_e$
$U_{\max}$: Maximum cylinder velocity
U_∞ : Free stream velocity
u : Velocity component of fluid in x-direction
u_{cyl} : Velocity component of cylinder in x-direction
$u_{i,j}$: Velocity at grid point (i, j)
$u(x_s)$: Velocity at immersed boundary point
$V(x_s, t)$: Boundary velocity
v : Velocity component of fluid in y-direction
v_{cyl} : Velocity component of cylinder in y-direction

* Corresponding Author,
E-mail : myha@pusan.ac.kr
TEL : +82-51-510-2440; **FAX** : +82-51-512-9835
Department of mechanical engineering, Pusan National University, Busan 609-735, Korea. (Manuscript **Received** August 26, 2005; **Revised** March 23, 2006)

x_s : Discrete immersed boundary point
x_{cyl} : Position of cylinder in x-direction
y_{cyl} : Position of cylinder in y-direction

Greek symbols

α : Negative gain of momentum forcing
β : Negative gain of momentum forcing
ν : Kinematic viscosity

Superscripts

n : Time step
$*$: Intermediate level velocity

Subscripts

cyl : Cylinder
e : Oscillation
i : Grid point index, x-direction
j : Grid point index, y-direction
m : Modulation
max : Maximum
o : Fixed cylinder
s : Discrete immersed boundary point
∞ : Free stream

1. Introduction

One of the main issues of computational fluid dynamics is handling complex geometries and moving bodies. The numerical simulations have lagged the experiments during the last decades due to the difficulties in treating complex geometries and moving bodies numerically. Although the few numerical simulations have well represented the global results observed by the experiments, there is still much work to do in order to simulate more complicated configurations. Recently, new methodologies have been developed to overcome the difficulty of generating specially fitted surfaces to the complicated shapes of bodies. Among such techniques, the immersed boundary method (IBM) has shown promising results.

The immersed boundary method (IBM) refers to the imposing of body forces on set of grid points at or inside the body surface. Such forces are to bring the fluid velocities to wall velocities at the points coinciding with surface location. Since the surface in general does not coincide with the computational grid points, the forces in that case are to generate artificial velocities to the grid points enclosed inside the body to those outside the body so as to bring the interpolated velocity at the surface closer as much as possible to wall velocities. Details of the method can be found in Saiki and Birigen (1996) gave a detail explanation for the IBM method and summarized collaborative researches over thirty years, mainly in the biological fluid dynamics.

Two forms of the acting force have been proposed so far ; the feedback forcing and the direct forcing. The former method has been used by Peskin (1982), Goldstein et al.(1993, 1995), Goldstein and Tuan (1998), Saiki and Biringen (1996), and Lee (2003). Peskin (1982) used momentum forcing to simulate the flow in moving heart on Cartesian grid. Goldstein and his co-authors (1993, 1995, 1998) used a spectral code to mimic somehow scalloped shape riblets. Although, their method showed reasonable results, the appropriateness of it to more complicated shapes seems questionable in the light of the severe limitation of time step. On the other hand, since the forces are applied on the grid points, the exact simulation of surfaces which do not coincide exactly with the computational grid points pushes the method to suffer from the interpolation deficiency. This difficulty becomes more pronounced when the pressure or viscous forces at the surfaces are desired since the surface location is not well determined. Lee (2003) analyzed stability of Saiki and Biringen's (1996) method and found that the linear interpolation of the virtual boundary velocity and subsequent spreading of the virtual forcing relax the time-step limit for stability up to four times. Through his analysis, critical disadvantage for large time-step limit for stability in feedback method could be overcome.

The alternative approach for the forcing is the direct method which determines the forces from the balance of the discretization equations after imposing the desired velocities in the inertial term. This method has been widely implemented with different schemes, for example, Mohd-Yusof (1997) used it with B/Spline Fourier pseudospec-

tral transform; Fadlun et al.(2000) used it FD technique for 3D complex geometries; Verzicco et al.(2000) presented a LES of moving boundaries which mimic the motion of the internal combustion engine piston; Kim et al.(2001) introduced mass sink/source in the continuity equation to satisfy no-slip condition on the immersed boundary and used FV approach to simulate the flow over cylinder and sphere.

Aside from the implementation of momentum forces at grid points, Ye et al.(1999) and Udaykumar et al.(1997, 2001) proposed a different approach in order to simulate complex geometry inside the Cartesian domains. In Ye et al.(1999)'s method, the control volumes near the immersed boundaries are reformed to exclude the solid part of the cells containing the immersed body and including the fluid part. The resulting cells are in general reshaped in trapezoidal-like cells. Hence, interpolation schemes were developed to calculate the fluxes across the faces of the new constructed cells which retain the second-order spatial accuracy. Udaykumar et al.(1997) simulated multi phase flows and also applied it to moving bodies. Udaykumar et al.(2001) extended the method of Ye et al.(1999) and applied it to channel with moving wall, oscillating cylinder, deforming diaphragm problem.

The present study uses the feedback forcing method suggested by Saiki and Biringen (1996) in order to simulate flows around stationary and moving cylinders. To treat stationary single and multiple cylinders, the capability of feedback forcing method has been guaranteed by the comparison of versatile results of present study with those of previous experimental and numerical researches. Also, the horizontally oscillating cylinder in a stationary flow and vertically oscillating cylinder in a uniform flow are simulated to verify present adopted method for moving bodies. Those results were well compared with those of previous experiments and numerical study using moving grid technique. Feasibility study for IBM with feedback forcing has been carried out to two oscillating cylinders. Drag and lift coefficients are presented for two cylinders oscillating sinusoidally with phase difference of 180°.

2. Computational Details

2.1 Governing equations

The methodology of solving flows around stationary and moving cylinders using finite volume technique with the treatment of immersed bodies will be presented in this section.

Figure 1 shows the computational domains and coordinates systems for different cases considered in this study. The integral form of the governing equations describing instantaneous incompressible viscous flow in a dimensionless form is given by the continuity and the momentum equations as follows;

$$\int_{cs} \vec{u}.\hat{n}\, ds = 0 \tag{1}$$

$$\frac{\partial}{\partial t}\int_{cv} \vec{u}\, dV + \int_{cs} \vec{u}(\vec{u}.\hat{n})\, dS = -\int_{cs} p\hat{n}\, dS + \frac{1}{\mathrm{Re}}\int_{cs} \nabla \vec{u}.\hat{n}\, dS \tag{2}$$

where $\hat{n}$ is the unit vector normal to the control volume surface and $\vec{u}=(u, v)$ the velocity vector whose components are in x- and y-directions, respectively.

The normalization of above equations using cylinder diameter D and free stream velocity U_∞ results in dimensionless parameter of Reynolds number, $\mathrm{Re}=U_\infty D/v$. For inline oscillation $\mathrm{Re}=U_{\max}D/v$ is used and $U_{\max}$ is the maximum cylinder speed. The equations are discretized on non-staggered Cartesian grids. A second-order accurate finite volume method is used in the present study where the second-order two-step fractional step method is employed for time advancement. The scheme was used previously by Kim and Moin (1985) and Zang et al.(1994). In this time stepping scheme, the velocity is advanced from time level 'n' to an intermediate level '$*$' by solving the advection-diffusion equation without pressure term in which the nonlinear terms are treated explicitly using second-order Adams-Bashforth scheme. The diffusion terms are treated implicitly using Crank-Nicolson scheme. Therefore the semi-discrete form of the advection-diffusion equation can be written as;

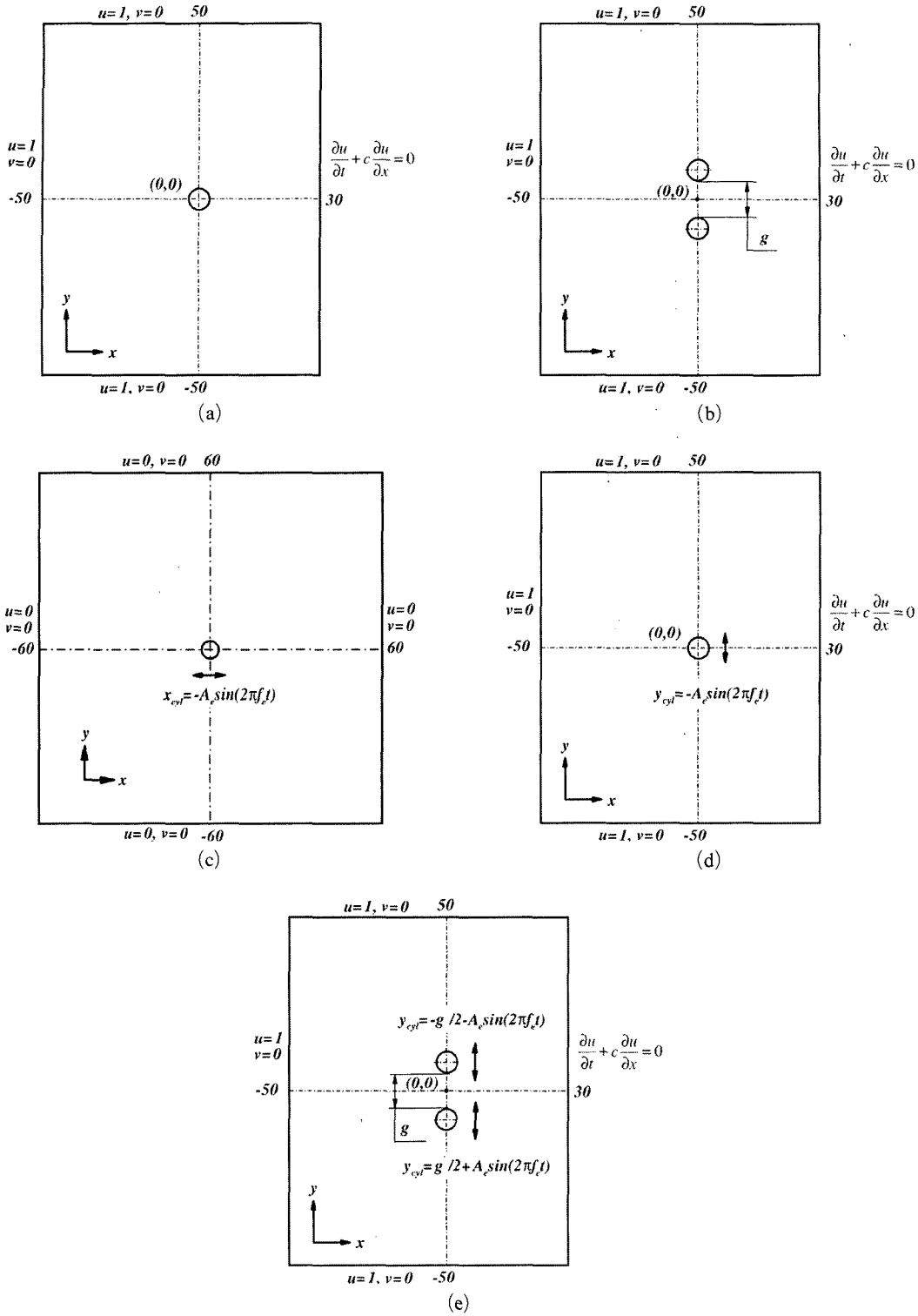

Fig. 1 Schematic diagram for computational domain and coordinate systems (a) one fixed cylinder, (b) two fixed cylinders, (c) inline oscillating cylinder, (d) one cross-flow oscillating cylinder, (e) two cross-flow oscillating cylinders

$$\int_{CV}\frac{u^*-u^n}{\Delta t}dV+\frac{1}{2}\int_{CS}[3u^n(u^n.\hat{n})-u^{n-1}(u^{n-1}.\hat{n})]\,dS$$
$$+\frac{1}{2\,\mathrm{Re}}\int_{CS}(\nabla u^*+\nabla u^n).\hat{n}\,dS \tag{3}$$

The velocity boundary condition imposed in the above equation uses the velocity at the full time step corresponding to u^{n+1}. Following the advection-diffusion step, the pressure correction can be done by satisfying the integral mass conservation equation given by

$$\int_{CS}(u^{n+1}.\hat{n})\,dS=0 \tag{4}$$

then the pressure correction step

$$\int_{CS}\frac{u^{n+1}-u^*}{\Delta t}\,dV=-\int_{CV}\nabla p^{n+1}dV \tag{5}$$

results in the following Poisson equation.

$$\int_{CS}(\nabla p^{n+1}).\hat{n}\,dS=\frac{1}{\Delta t}\int_{CS}(u^*.\hat{n})\,dS \tag{6}$$

After getting the pressure, u^{n+1} is calculated from the resulting pressure field as follows;

$$u^{n+1}=u^*-\Delta t\,(\nabla p^{n+1}) \tag{7}$$

2.2 Immersed boundary method

2.2.1 Interpolation scheme

Generally, immersed boundary does not coincide with grid points. So, interpolation is needed for immersed boundary value between grid points. Peskin (1982) used first-order cosine function for interpolation and extrapolation. Goldstein (1993) interpolated velocities of grid points from immersed boundary points with spectral interpolation and extrapolated forcing term of immersed boundary points from grid points with linear interpolation. Saiki and Biringen (1996) used bilinear interpolation that is also first-order accurate.

In this study, bilinear interpolation is used to know surface velocities with its position information. The discrete surface points in Fig. 2 are immersed boundary points, x_s. So, velocity of immersed boundary point $u(x_s)$ is interpolated from velocities, $u_{i,j}$ at near by grid points.

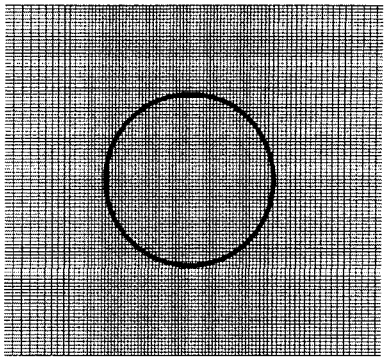

(a) Full cylinder body

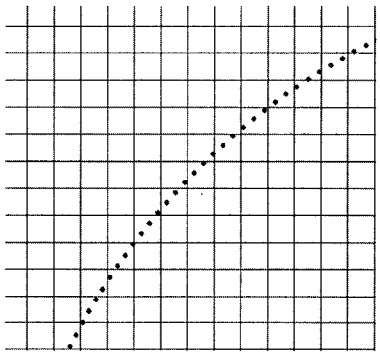

(b) Upper left portion of the cylinder

Fig. 2 Superposition of the immersed boundary points on the computational grid

- Bilinear interpolation scheme

$$u(x_s)=\sum_{i,j}^{i+1,j+1}D_{ij}(x_s)\,u_{i,j} \tag{8}$$

where

$$D_{i,j}(x_s)=d(x_s-x_i)\,d(y_s-y_j) \tag{9}$$

In Eq. (9),

$$d(x_s-x_i)=\frac{(x_s-x_i)}{(x_{i+1}-x_i)}\ \text{if}\ x_i<x_s \tag{10a}$$

$$d(x_s-x_i)=\frac{(x_s-x_i)}{(x_i-x_{i-1})}\ \text{if}\ x_i>x_s \tag{10b}$$

and

$$d(x_s-x_i)=1\ \text{if}\ x_i=x_s \tag{10c}$$

2.2.2 Feedback momentum forcing

In implementing the method of Saiki and Biringen (1996), no-slip condition is satisfied with a feedback forcing function which is added

Table 1 Numerical examples and details

Case	Cylinder	Re	Grid number
1	One stationary cylinder	40, 100, 120, 185	336×381
2	Two stationary cylinders, side-by-side arrangement	40, 100	336×381
3	One cylinder, inline oscillation	100	331×271
4	One cylinder, cross flow oscillation	185	336×381
5	Two cylinders, side-by-side arrangement, cross flow oscillation	185	336×381

to the momentum equations. This feedback momentum forcing function, $f(X_s, t)$ can be expressed as

$$F(x_s, t)=\alpha\int_0^t[u(x_s, t')-V(x_s, t')]dt' +\beta[u(x_s, t)-V(x_s, t)] \quad (11)$$

Here the coefficients of α and β are big negative constants and they have $[1/T^2]$ and $[1/T]$ dimension, respectively. α term has role to produce oscillations and β term to dampen the oscillations. α and β are flow dependent constants and there is no general rule to determine them. $V(X_s, t)$ is boundary velocity and if the boundary is fixed, it is zero for no-slip condition. Deforming, rotation and moving bodies can be simulated by varying $V(X_s, t)$ adequately. Velocity difference, actually error, $u(X_s, t)-V(X_s, t)$ determines the feedback forcing and it is the momentum forcing that controls boundary velocity, u to be same with desired velocity $V(X_s, t)$.

If the boundary does not rotate or move, $V(X_s, t')$ and $V(X_s, t)$ becomes "0" and Eq. (11) becomes Eq. (12). Time integral is replaced with Riemann sum, Eq. (13), we get Eq. (14) for feedback momentum forcing.

$$F(x_s, t)=\alpha\int_0^t[u(x_s, t)]dt'+\beta[u(x_s, t)] \quad (12)$$

$$\int_0^t u(x_s, t')\,dt'\approx\sum_{j=1}^{N}u(x_s, j)\Delta t \quad (13)$$

$$F(x_s, t)=\alpha\sum_{t'=0}^{t'=t}u(x_s, t')+\beta[u(x_s, t)] \quad (14)$$

With Eq. (14) forcing density, $F(x_s, t)$ at immersed boundary is calculated and re-distributed to grid points near immersed boundary again. Sum of nearby forcing density multiplied by weighting factor is the momentum forcing, f of nearby grid point. The weighting factor is given from the interpolation scheme.

$$f=\frac{1}{n}\sum_{n=1}^{N_b}D_{i,j}(x_s)F(x_s) \quad (15)$$

Here, n is the number of immersed boundary points that affect the grid point. The method prescribed above is 'area-weighted' method by Saiki and Biringen (1996).

2.3 Numerical conditions

The application cases of IBM with feedback forcing considered in this study and mesh resolutions for different cases are listed in Table 1. The minimum grid spacing in the vicinity of the cylinder for all cases was $\Delta x_{min}=\Delta y_{min}=0.02$ and clustered coarse grid was used far from cylinder. At the inflow and outflow, uniform flow conditions and convective conditions are assumed, respectively. At the upper and lower boundaries, shear free conditions are imposed as shown in Fig. 1.

Except inline oscillation, f_o is the Strouhal number of one fixed cylinder at same Re and f_e is oscillation frequency of cross flow and inline oscillation.

For stationary cylinder flow used $\alpha=-3000$ and $\beta=-40$ and $\alpha=-20000$ and $\beta=-100$ for oscillating cylinder flow.

3. Results

3.1 Single stationary cylinder

Lai and Peskin (2000) showed several methods to calculate drag and lift forces of body implemented by immersed boundary methods. In this

Table 2 Drag and lift coefficients for over a fixed circular cylinder

	Re	C_D	C'_L	St
Present	40	1.53		
	100	1.33	0.28	0.166
	120	1.32	0.36	0.173
Kim et al. (2003)	40	1.51		
	100	1.33	0.32	0.165
Park et al. (1998)	40	1.51		
	100	1.33	0.33	0.165
	120	1.32	0.41	0.175

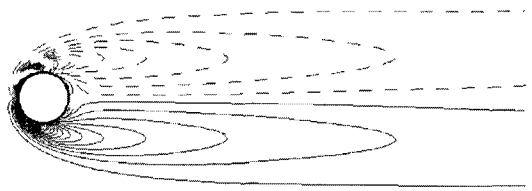

(a) Re=40

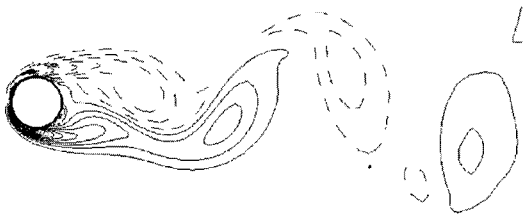

(b) Re=100

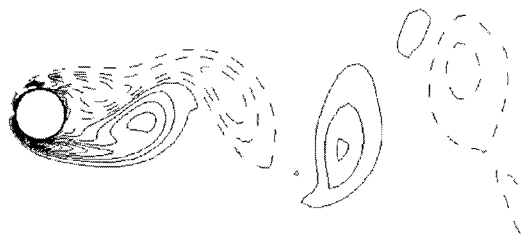

(c) Re=120

Fig. 3 Spanwise vorticity contours near a circular cylinder

study, for the stationary flow, drag and lift forces are evaluated by integrating applied momentum forcing. Drag and lift coefficients and Strouhal number were compared in Table 2. Both of coefficients at corresponding Reynolds number are in good agreement with Kim et al.(2001) using direct IBM and Park et al.(1998) using body-fitted mesh. Also, present Strouhal numbers at different Reynolds numbers agree well with those

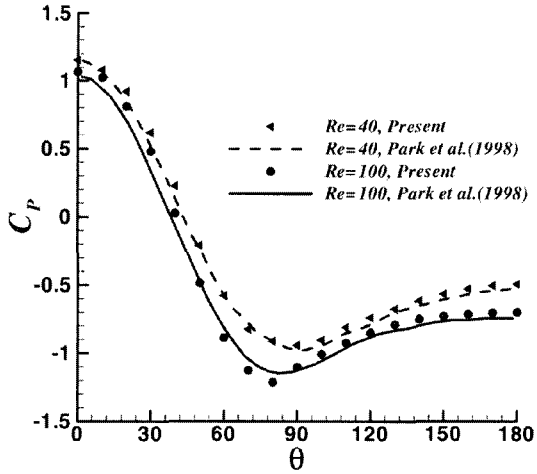

Fig. 4 Wall pressure coefficients along the cylinder surface

of previous studies.

Instantaneous spanwise vorticity contours in Fig. 3 clearly show the flow dependency on Reynolds number. As well known, the flow around single stationary cylinder at Re=40 is characterized by steady symmetric separation bubble and unsteady Karman vortex street dominates in wake region for Re=100 and 120.

Figure 4 shows the comparison of present pressure coefficient with that of Park et al.(1998) obtained by a body-fitted mesh. Present pressure coefficients at Re=40 and 100 obtained by feedback IBM well represent high resolution numerical results of Park et al.(1998).

3.2 Two stationary cylinders in a side-by-side arrangement

The flow over two circular cylinders in a side-by-side arrangement was simulated by using feedback IBM. Generally, there are two non-dimensional variables that govern the flow over two cylinders in a side-by-side arrangement. One is the Reynolds number and another is the dimensionless gap between two cylinders.

Flow over two cylinders in a side-by-side arrangement was studied by Zdravkovich (1997), Sumner et al.(1999) and Williamson (1985). Recently, Kang (2003) examined, using direct IBM, Reynolds numbers and gap ranging of $40 \leq Re \leq 160$ and $g < 5$, respectively. Within the ranges of

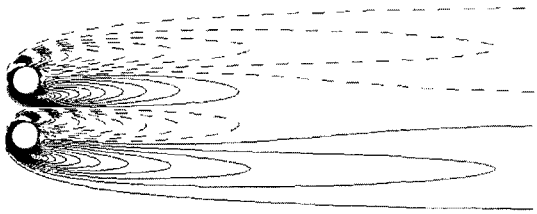

(a) Re=40 and g=1

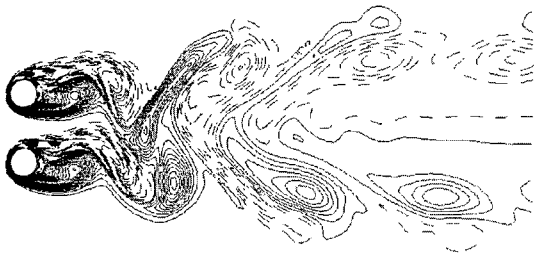

(b) Re=100 and g=1.5

Fig. 5 Spanwise vorticity of two fixed cylinders

Re and g of Kang (2003), two cases of g=1 at Re=40 and g=1.5 at Re=100 are considered in this study to compare the results obtained by present feedback IBM with those of Kang (2003) using direct IBM.

Figure 5 shows wake patterns visualized by contours of spanwise vorticity at g=1 for Re=40 and g=1.5 for Re=100. The steady flow and apparently symmetric wake patterns about the centerline without vortex shedding can be observed in Fig. 5(a). Time histories of drag and lift coefficients at g=1 for Re=40 shows the steady state in Fig. 6(a), which can be comparable to Fig. 5(a).

In case of g=1.5 at Re=100, same wake pattern with vortex shedding in almost equal phase can be observed at both of upper and lower cylinders. Further downstream, vortices occurred at both cylinders start to merge as shown in Fig. 5 (b). Above wake patterns can be deducted from time histories of drag and lift coefficients in Fig. 6(b).

Before transition duration around t<50, lift coefficients of upper and lower cylinder are anti-phase (of 180° phase difference). After transition, even lift coefficients for both cylinders in-phase (of the same phase), the drag coefficients are out of phase. Thus, the flow structure is called the in-phase-synchronized wake pattern as observed in Kang (2003).

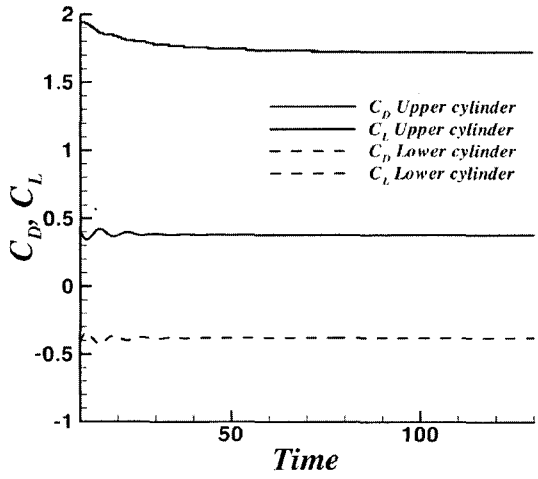

(a) Re=40 and g=1

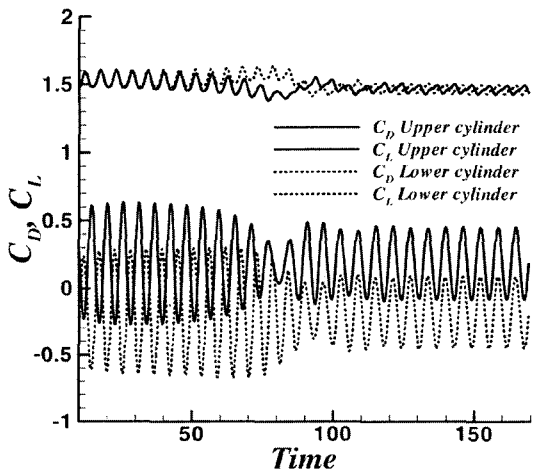

(b) Re=100 and g=1.5

Fig. 6 Time evolutions of the lift and drag coefficients according to the wake pattern

Table 3 Drag and lift coefficients for over two fixed circular cylinders

	case	$\overline{C}_D$	C_L (avg.)	St
Present	Re=40, g=1	1.73	0.38	
	Re=100, g=1.5	1.47	0.28	0.161
Kang (2003)	Re=40, g=1	1.7	0.37	
	Re=100, g=1.5	1.43	0.27	0.164

Averaged drag and lift coefficients are compared and agree well with Kang (2003) in Table 3. Such as those wake patterns and characteristics of drag and lift coefficients for two cases of g=1

at Re=40 and g=1.5 at Re=100 are in good agreement with Kang (2003). Also, present time-averaged drag and lift coefficients quantitatively agree well with those of Kang (2003) as shown in Table 3.

3.3 Inline oscillation

Inline oscillation of cylinder has been studied to understand flow and structure interaction. In this study, inline oscillation has been simulated by using feedback IBM and results were compared with those of Dütsch et al.(1998)'s experimental study and Guilmineau & Queutey (2002)'s numerical study.

Inline oscillation is characterized by two dimensionless parameters of Reynolds number, and Keulegan-Carpenter number (Keulegan, 1958). The trajectory of cylinder center and velocity of cylinder are imposed as $x_{cyl}(t) = -A_e \sin(2\pi ft)$ and $u_{cyl}(t) = -2\pi fA\cos(2\pi ft)$, respectively. So, Keulegan-Carpenter number is redefined as $KC = 2\pi A/D$. In present research, inline oscillation of cylinder with KC=5 at Re=100, which is the same condition of Dütsch et al.(1998) and Guilmineau & Queutey (2002), is calculated.

Figure 7 shows vorticity and pressure contours of instantaneous field at four different phase positions of 0°, 60°, 180° and 270°. When the phase position is between 0°~90°, we can see the cylinder is moving from right to left and decelerating in the pressure contour. At position 0° in Fig. 7(a), pressure at left side of cylinder is high and pressure at top and bottom of the cylinder is low. As cylinder decelerates, left side pressure increases. At position 60° in Fig. 7(b), it moves to left, however, right side pressure is higher than left side. This is because the fluid near the cylinder is faster than the decelerating cylinder. When the cylinder reaches at position 90°, it stops and restarts to move to right during position 90°~180°.

As the cylinder moves to left from right, a vortex pair is developing near the cylinder and separation takes place. When it comes to its extreme left position, phase position 90°, the cylinder stops and restarts to move in opposite direction.

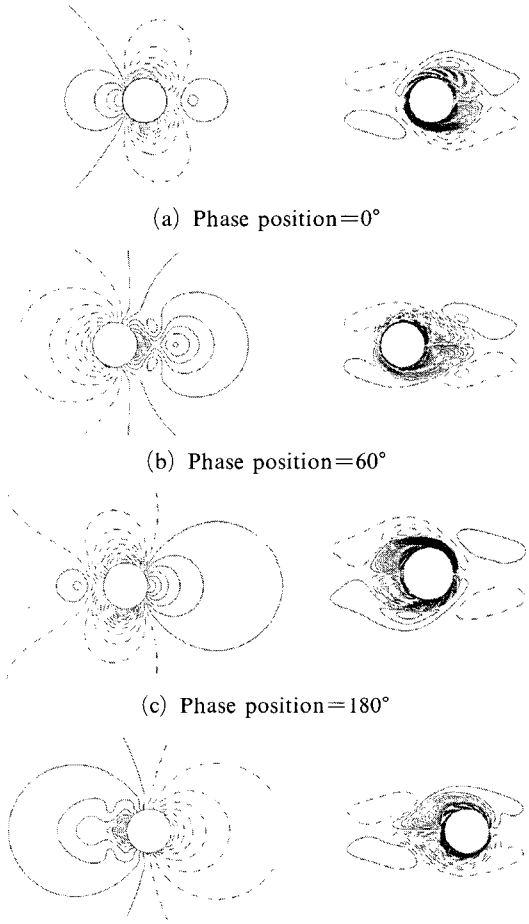

(a) Phase position=0°

(b) Phase position=60°

(c) Phase position=180°

(d) Phase position=270°

Fig. 7 Pressure and vorticity isolines (negative values dashed) at Re=100 and KC=5

In Fig. 7(d), again, another vortex pair begins to develop around the cylinder and it splits and goes through the counter rotating vortex pair that was made during previous right-to-left movement. The boundary layer merges with the vortex pair in front of the cylinder. In Fig. 7(d), the cylinder reaches at its extreme right position, phase position=270°. Another boundary layer is developing again, so the above motions happen periodically. These periodical inline motions obtained from this study agree very well with those of Dütsch et al.(1998) and Guilmineau & Queutey (2002).

As shown in Fig. 8, the flow fields around inline oscillating cylinder at three different phase angles of 180°, 210° and 330° are illustrated by streamlines obtained by experimental results from

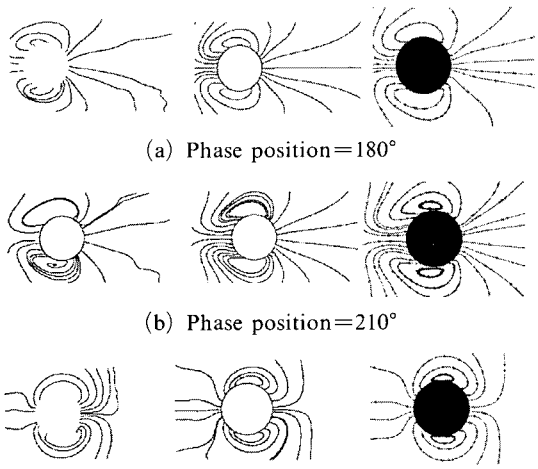

(a) Phase position=180°

(b) Phase position=210°

(c) Phase position=330°

Fig. 8 Measured Dütch et al.(1998) (left), Guilmineau & Queutey (2002) (center) and computed streamlines (right) in the vicinity of the cylinder at Re=100 and KC=5 at different phase positions

Dütsch et al.(1998), numerical results from Guilmineau & Queutey (2002) and present feedback IBM. These three different studies predicted almost identical flow fields.

For further quantitative comparison in Fig. 9, local phase-averaged velocities at three different phase angles corresponding to Fig. 8 are compared with numerical results of Guilmineau & Queutey (2002). Present velocity profiles at four locations for a constant x-position give good comparison with those of Guilmineau & Queutey (2002).

The time variation of inline force computed in Fig. 10 fits well with that of Guilmineau & Queutey (2002). But both results from present and Guilmineau & Queutey (2002) have discrepancy with Morison equation (Chakrabarti, 1987) around phase positions, t/T_e=0.3 and 0.8.

3.4 Cross-flow oscillation

In present research, the cross-flow oscillation of single cylinder is calculated for Re=185, A_e/D=0.2 and two cases of f_e/f_o=0.8 & 1.1 according to numerical results of Guilmineau & Queutey (2002). The trajectory of cylinder center along y-direction is imposed as $y_{cyl}(t) = -A_e \sin(2\pi f_e t)$ based on Guilmineau & Queutey (2002)'s study.

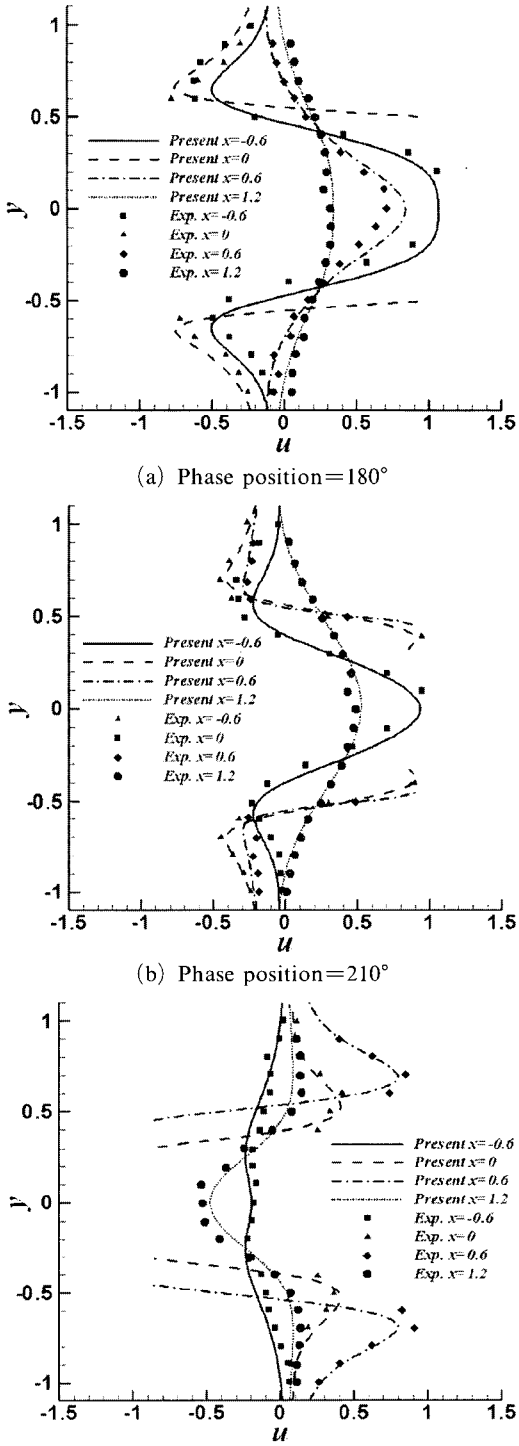

(a) Phase position=180°

(b) Phase position=210°

(c) Phase position=330°

Fig. 9 Comparison of U component at Re=100 and KC=5 between present computation and experimental investigation Dütsch et al.(1998) at four cross-sections with constant x-value

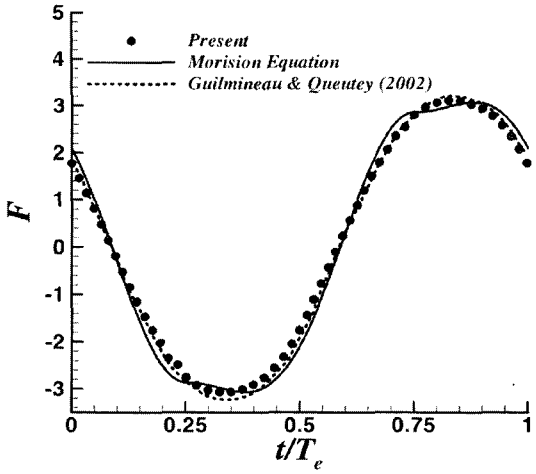

Fig. 10 Comparison of the dimensionless in-line force among present, Morison equation and Guilmineau & Queutey (2002)'s computation at Re=100 and KC=5

Table 4 Drag and lift coefficients for over a fixed circular cylinder at Re=185

Re=185	$\overline{C}_D$	C_{Lrms}	St
Present	1.31	0.44	0.191
Guilmineau & Queutey (2002)	1.29	0.44	0.195

Table 5 Drag and lift coefficients for cross flow oscillation at Re=185

	f_e/f_o	$\overline{C}_D$	C_{Lrms}
Present	0.8	1.19	0.11
Guilmineau & Queutey (2002)		1.22	0.1
Present	1.1	1.38	0.76
Guilmineau & Queutey (2002)		1.37	0.87

First, the natural shedding frequency from the stationary cylinder, f_o of present result is compared with that of Guilmineau & Queutey (2002) in Table 4, which is in good agreement. Also, the satisfactory result of comparison of time-averaged drag and RMS lift coefficients with present results and Guilmineau & Queutey (2002) can be seen in Table 5.

Figure 11 shows the time evolutions of drag and lift coefficient for f_e/f_o=0.8 and 1.1. The beating frequency decreases with excitation frequency (f_e) increasing. In both cases, drag coefficient has same frequency with excitation frequency, which suggests that the excitation frequency dominates the flow in lock-in regime. In case of f_e/f_o=1.1 as shown in Fig. 11(b), it has modulation phenomenon which is not shown in f_e/f_o=0.8 case. Both of drag and lift coefficients for f_e/f_o=1.1 show regular signs of the influence of a higher harmonic. These results well reproduced the numerical results of Guilmineau & Queutey (2002).

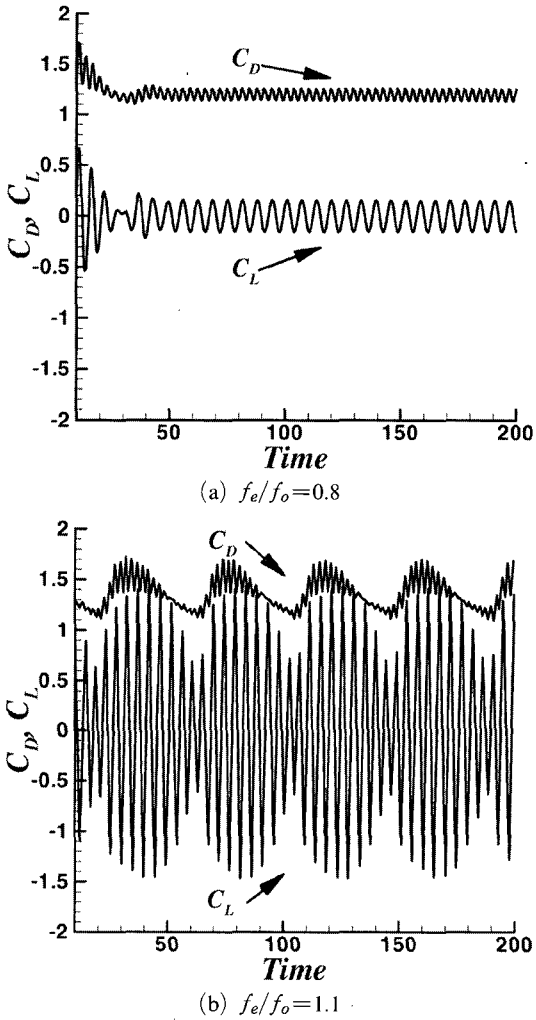

Fig. 11 Time evolutions of the lift and drag coefficients according to the wake pattern at Re=185

The good agreement between present results and numerical results of Guilmineau & Queutey (2002) is shown by the comparisons of flow fields

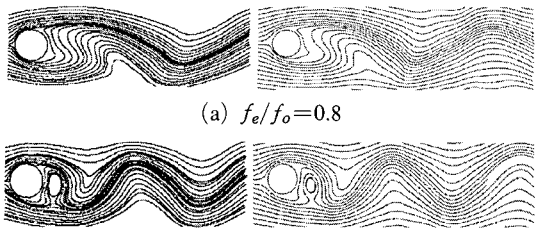

(a) $f_e/f_o=0.8$

(b) $f_e/f_o=1.1$

Fig. 12 Instantaneous streamlines. In all frames, the location of the cylinder is at its extreme upper position at Re=185, Guilmineau & Queutey (2002) (left) and present result (right)

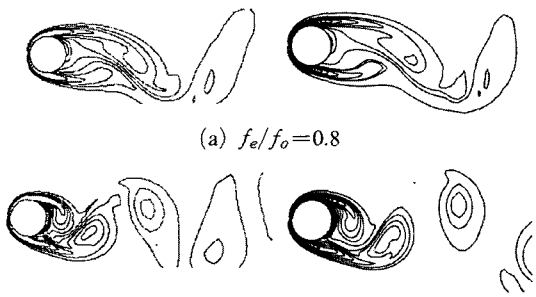

(a) $f_e/f_o=0.8$

(b) $f_e/f_o=1.1$

Fig. 13 Instantaneous vorticity contours. In all frames, the location of the cylinder is at its extreme upper position at Re=185, Guilmineau & Queutey (2002) (left) and present result (right)

visualized by streamlines and spanwise vorticity in Figs. 12 and 13. As expected, $f_e/f_o=1.1$ case has stronger vorticity and more frequent vortex shedding than $f_e/f_o=0.8$.

Figure 13 shows the comparison of pressure coefficient with result from Guilmineau & Queutey (2002), where the cylinder is at its extreme upper position and the x-coordinate indicates the angle from front in clockwise direction.

3.5 Two-oscillating cylinders

In this study, two oscillating cylinders are simulated by using same conditions of $A_e/D=0.2$ and f_e/f_o with those of previous cross flow oscillation. The two cylinders oscillate as Eqs. (16) and (17), respectively.

$$y_{cyl,up}(t)=g/2+A_e\sin(2\pi f_e t) \tag{16}$$

$$y_{cyl,dn}(t)=-g/2-A_e\sin(2\pi f_e t) \tag{17}$$

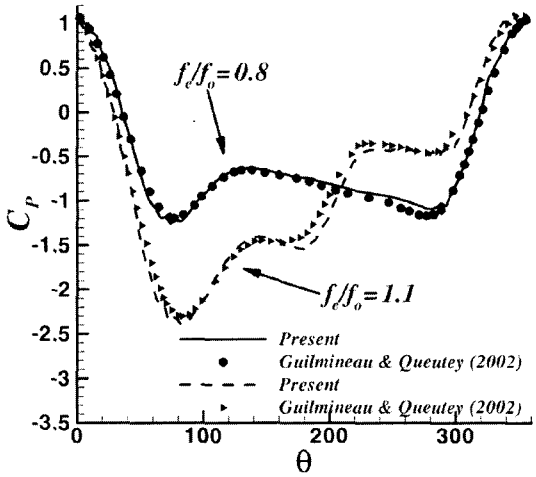

Fig. 14 Wall pressure coefficients along the cylinder surface. The location of the cylinder is at its extreme upper position at Re=185

Where, '*up*' designates upper cylinder and '*dn*' lower cylinder. The dimensionless gap of two cylinders g is in between 2 and 2.8.

Figure 15 shows the vorticity contours and streamlines when the upper cylinder is at extreme upper position and the lower cylinder at extreme lower position ($g=2.8$). Two-cylinder oscillation has closed streamlines which are not seen in one-cylinder oscillation at same frequency ratio. In Fig. 16, drag and lift coefficient is plotted as a function of time and modulation phenomenon also can be found in the case of one-oscillating cylinder at $f_e/f_o=1.1$. According to Kang (2003), even though it is on fixed cylinders, this two-oscillating cylinder case may be in mixed pattern of flip-flop and deflected pattern. g varying with oscillating cylinders is one of the parameters that determine the regime of wake pattern. Two cylinders seem to cross the border for flip-flop and deflected pattern repetitively.

Velocity spectra in Fig. 17 are measured at $x=2$, $y=\pm4$. The velocity spectra at upper point ($x=2$, $y=4$) shows the dominance of natural frequency but at the lower point, excitation frequency is stronger than natural frequency. Series of modulation frequency and the difference of oscillating frequency and modulation frequency (f_e-f_m) have peak values in Fig. 17. As subharmonic response with $f_e\approx4f_m$ is observed and

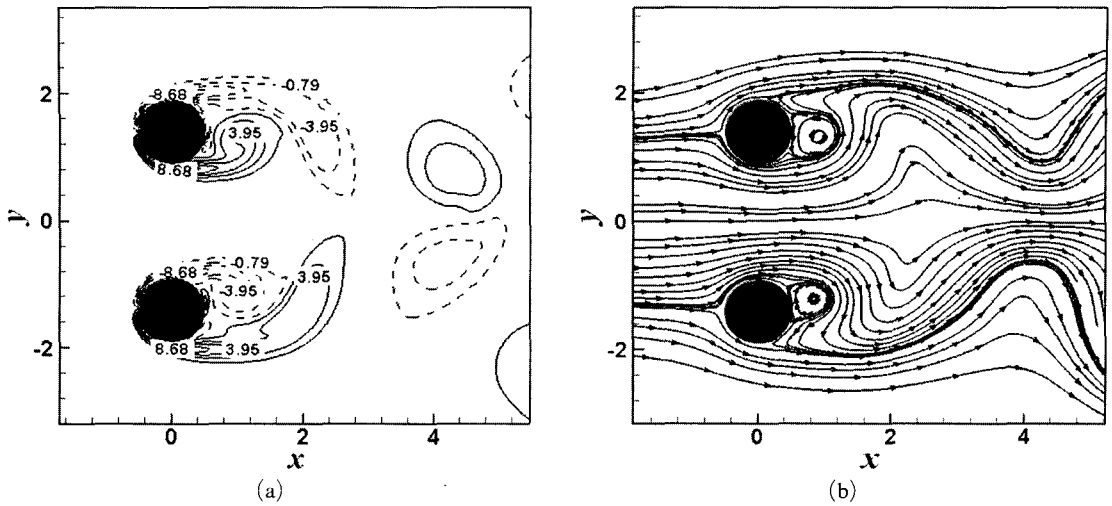

Fig. 15 (a) Instantaneous vorticity contours and (b) streamline of two-oscillating cylinders at $f_e/f_o=0.8$, $g=2.8$

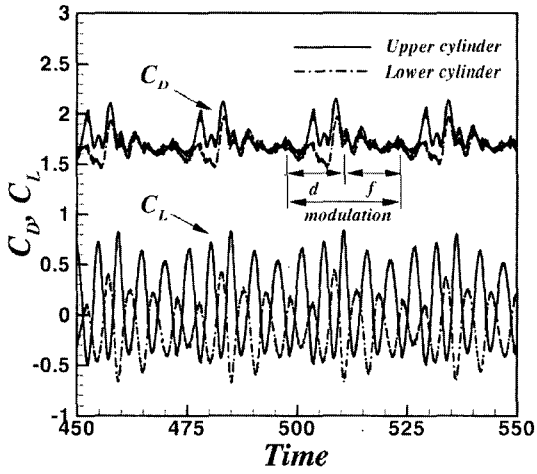

Fig. 16 Drag and lift coefficient as a function of time. 'd' and 'f' mean deflected pattern and flip-flop pattern respectively

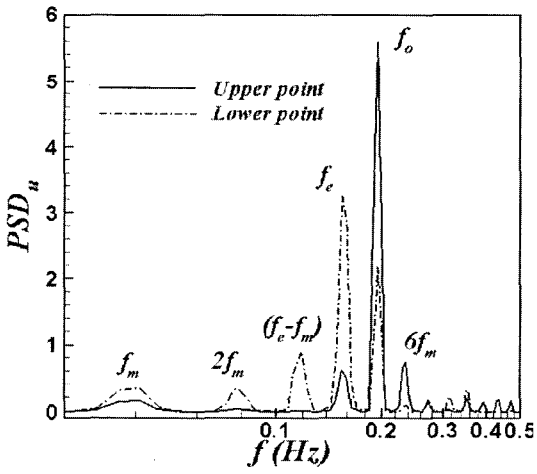

Fig. 17 Velocity spectra taken at $x=2$, $y=4$ (upper point) and $x=2$, $y=-4$ (lower point)

the exciting frequency is not dominant, this case is regarded as in non-lock-in regime.

4. Conclusions

Feedback immersed boundary method is applied to stationary and oscillating cylinders flow. To validate, one and two fixed cylinders are simulated. Pressure coefficient, wake pattern and drag & lift coefficients are presented and compared with previous results. Inline oscillation and cross flow oscillation are considered for moving-body application. As well as flow pattern, detailed velocity profile and drag & lift coefficients are described. For cross flow oscillation, the cases of $f_e/f_o=0.8$ and $f_e/f_o=1.1$ at Re=185 are verified to be in lock-in regime.

For further application, immersed boundary method is applied to two independently moving cylinders in uniform flow. At Re=185, $A_e/D=0.2$, $f_e/f_o=0.8$, $g=1.2$, two oscillating cylinder flow has asymmetric flow pattern, modulation

phenomenon and vortex roll-up that are not seen one-cylinder oscillation at same Re and frequency ratio. In velocity spectra obtained in the wake region, several peaks are found and that peaks are related with modulation, natural and excitation frequency.

Acknowledgments

This work was supported by Advanced Ship Engineering Research Center (ASERC), Pusan National University, through the Korean Science and Engineering Foundation.

References

Chakrabarti, S. K. 1987, "Hydrodynamics of Offshore Structures," Computational Mechanics Publications.

Dütsch, H., Durst, F., Becker, S. and Lienhart, H., 1998, "Low-Reynolds-number Flow around an Oscillating Circular Cylinder at Low Keulegan-Carpenter Numbers," *J. Fluid Mech.*, Vol. 360, pp. 247~271.

Fadlun, E. A., Verzicco, R., Orlandi, P. and Mohd-Yusof, J., 2000, "Combined Immersed Boundary Finite-Difference Methods for Three-Dimensional Complex Flow Simulations," *J. Comput. Phys.*, 161, pp. 35~60.

Goldstein, D., Handler, R. and Sirovich, L., 1993, "Modeling a No-Slip Boundary with an External Force Field," *J. Comput. Phys.*, 105.

Goldstein, D., Handler, R. and Sirovich, L., 1995, "Direct Numerical Simulation of Turbulent Flow over a Modeled Riblet-Covered Surface," *J. Fluid. Mech.*, 302, pp. 333~376.

Goldstein, D. and Tuan T.-C., 1998, "Secondary Flow Induced by Riblets," *Journal of Fluid Mechanics*, Vol. 363, pp. 115~151.

Guilmineau, E. and Queutey, P., 2002, "A Numerical Simulation of Vortex Shedding from an Oscillating Circular Cylinder," *J. Fluids and Structures*, Vol. 16, No. 6, pp. 773~794

Kang, S., 2003, "Characteristics of Flow over Two Circular Cylinders in a Side-by-side Arrangement at Low Reynolds Numbers," *Phys. Fluids*, Vol. 15, No. 9, pp. 2486~2498.

Keulegan G. H. and Carpenter, L. H., 1958, "Forces on Cylinders and Plates in an Oscillating Fluid," *J. Res. Natl. Bur. Stand.*, 60, pp. 423~440.

Kim, J., Kim, D. and Choi, H., 2001, "An Immersed Boundary Finite-Volume Method for Simulation of Flow in Complex Geometries," J. Comput. Phys., 171, pp. 132~150.

Kim, J. and Moin, P., 1985, "Application of a Fractional-Step Method to Incompressible Navier-Stockes Equation," J. Comput.

Lai, M. C. and Peskin., C. S., 2000, "An Immersed Boundary Method with Formal Second-Order Accuracy and Reduced Numerical Viscosity," *J. Comput. Phys.*, 160, pp. 705~719.

Lee, C., 2003, "Stability Characteristics of the Virtual Boundary Method in Three-dimensional Applications," *J. Comput. Phys.*, 184, pp. 559~591.

Mohd-Yusof, J., 1997, "Combined Immersed Boundaries/B-Splines Methods for Simulations of Flows in Complex Geometries," *CTR Annual Research Briefs, NASA Ames/Stanford University*, pp. 317~327.

Park, J., Kwon, K. and Choi, H., 1998, "Numerical Solutions of Flow past a Circular Cylinder at Reynolds Numbers up to 160," *KSME Int. J.*, Vol. 12, No. 6, pp. 1200~1205.

Peskin, C. S., 1982, "The Fluid Dynamics of Heart Valves: Experimental, Theoretical, and Computational Methods," *Annu. Rev. Fluid Mech.*, 14, 235.

Saiki, E. M. and Biringen, S., 1996, "Numerical Simulation of a Cylinder in Uniform Flow; Application of a Virtual Boundary Method," *J. Comput. Phys.*, 123, pp. 450~465

Sumner, D. and Wong, S. S. T., Price, S. J. and Paidoussis, M. P., 1999, " Fluid Behavior of Side-by side Circular Cylinders in Steady Cross-flow," *J. Fluids Struct.*, Vol. 13, pp. 309~338.

Udaykumar, H. S., Kan, Heng-Chuan, Shyy, W. and Roger Tran-Son-Tay, 1997, "Multiphase Dynamics in Arbitrary Geometries on Fixed Cartesian Grids," *J. Comput. Phys.*, Vol. 137, pp. 366~405.

Udaykumar, H. S., Mittal, R., Rampunggoon, P. and Khanna, A., 2001, "A Sharp Interface

Cartesian Grid Method for Simulating Flows with Complex Moving Boundaries," *J. Comput. Phys.*, Vol. 174, pp. 345~380.

Verzicco, R., Mohd-Yusof, J., Orlandi, P. and Haworth, D., 2000, "Large Eddy Simulation in Complex Geometries Configurations Using Boundary Body Forces," *AIAA Journal*, Vol. 38, No. 3, pp. 427~433.

Williamson, C. H. K., 1985, "Evolution of a Single Wake behind a Pair of Bluff Bodies," *J. Fluid Mech.*, Vol. 159, pp. 1-18.

Ye. T., Mittal, R., Udaykumar, H. S. and Shyy, W., 1999. "An Accurate Cartesian Grid Method for Viscous Incompressible Flows with Complex Immersed Boundaries," *J. Comput. Phys.*, 156 , pp. 209~240.

Zang, Y., Street, R. L. and Koseff, J. R., 1994, "A Non-staggered Grid, Fractional Step Method for Time-Dependent Incompressible Navier-Stokes Equations in Curvilinear Coordinates," *J. Comput. Phys.*, 114, pp. 18~33.

Zdravkovich, M. M., 1997, "Review of Flow Interference between Two Circular Cylinders in Various Arrangements," *J. Fluids Eng.*, Vol. 99, pp. 618~633.